Study of the Density Distributions and Elastic form Factors of the Exotic Nuclei, ^{8}He And ^{26}F, Via the Three-Body Model

Ghufran M. Sallh, Ahmed N. Abdullah

Department of Physics, College of Science, University of Baghdad, Baghdad, Iraq

Abstract

   The matter, proton, and neutron density distributions of the ground state, the nuclear root-mean-square (rms) radii, and the elastic form factors of a two- neutron, ^{8}He and ^{26}F, halo nuclei have been studied by the three body model of $(core + 2n)$ within the harmonic oscillator (HO) and Woods-Saxon (WS) radial wave functions. The calculated results show that the two body model within the HO and WS radial wave functions succeeds in reproducing the neutron halo in these exotic nuclei. Moreover, the Glauber model at high energy (above several hundred MeV) has been used to calculate the rms radii and reaction cross sections of these nuclei.

Keywords: Exotic nuclei, elastic form factors, two neutrons halo nuclei.

دراسة توزيعات الكثافة وعوامل التشكل المرنة للنوى الغريبة He^8 و F^{26} باستخدام أنموذج الثلاث جسيمات

غفران مهدي صالح ، أحمد نجم عبدالله

قسم الفيزياء، كلية العلوم، جامعة بغداد، بغداد، العراق

الخلاصة

تم دراسة توزيعات الكثافة الكتلية ، البروتونية و النيوترونية وانصاف الاقطار النووية وعوامل التشكل لنوى He^8 وF^{26} باستخدام أنموذج الثلاث جسيمات مع الدوال الموجية لجهدي المتذبذب التوافقي وودز – ساكسون. وفقا للنتائج المحسوبة وجد ان هذا الانموذج يعطي وصفاً جيدا للتركيب النووي لنوى الهالة تحت الدراسة. كما تم استخدام نموذج جلوبر عند الطاقات العالية لدراسة المقاطع العرضية للتفاعل وانصاف النووية لهذه النوى.

1. Introduction

   One of the most exciting discoveries in the recent experimental progress using radioactive nuclear beams is the neutron halo in some light neutron-rich nuclei [1,2]. On the other hand, the search for proton halo in light proton-rich nuclei has attracted much attention in recent years. The theory, based on the relativistic mean filed (RMF) approximation, predicts the existence of proton halo or proton skin structure in some proton-rich nuclei [3,4] and experiments have subsequently observed some of the theoretical predictions [5,6].

   The observed neutron halo nuclei, such as ^{11}Li, ^{11}Be, ^{14}Be and ^{17}B, are in their ground state and are located near the drip line. In principle, the neutron halo appears in a very loosely bound nuclear

_____

*Email: ghufranmahdy@yahoo.com

system and with a low density, which results in substantially large spatial extension of the wave function for the neutron (proton) halo in these nuclei [7].

It is well known that a Glauber model analysis on reaction cross section is an important and feasible tool to deduce the nuclear size, which directly connects the reaction cross section to the nuclear density distribution. The Glauber theory in the optical limit approximation (OLA), which ignores any correlations between particles in the projectile or target, was successfully applied to describe unstable nucleus- nucleus scattering [8].

Alzubadi *et al*. [9] calculated the mass density distributions, the associated nuclear radii, and elastic electron scattering form factors of light exotic nuclei, namely ^{11}Li, ^{11}Be, ^{14}Be and ^{8}B, using shell model (SM) and Hartree–Fock (HF) methods. They considered truncated *spsdpf* no-core SM and WBP two-body effective interaction to give the SM wave functions. The single-particle matrix elements were calculated with Skyrme–Hartree–Fock (SHF) potential with different parametrizations. It was shown that the calculated densities and form factors are in fine agreement with experimental data. This agreement can be interpreted as the adequacy of the HF mean-field approximation for exotic nuclei. Abdullah [10] studied the ground state features, such as the proton, neutron, and matter densities, the rms nuclear proton, neutron, charge, and mass radii of unstable neutron-rich ^{14}B, ^{15}C, ^{19}C, and ^{22}N nuclei using the two body model of (core+n) within the radial wave functions of the cosh potential. The calculated results showed that the two body model with the radial wave functions of the cosh potential succeeds in reproducing neutron halo in these nuclei.

In this work, the Woods-Saxon (WS) and Harmonic Oscillator (HO) potentials wave functions within the three-body model of $(core + 2n)$ will be used to study the matter, proton, and neutron densities of the ground state, the nuclear root-mean-square (rms) radii, and elastic form factors of two-neutron, ^{8}He and ^{26}F, halo nuclei. Moreover, the Glauber model with an OLA will be used to calculate the matter rms radii and the reaction cross section (σ_R) of these nuclei.

2. Theory
The matter density distributions for unstable exotic nuclei are given as [11]:
$$\rho_m(r) = \rho_c(r) + \rho_v(r), \tag{1}$$
where $\rho_c(r)$ and $\rho_v(r)$ are the core and halo densities, respectively, and can be written as [10]:
$$\rho_c(r) = \frac{1}{4\pi}\sum_{n\ell} X_c^{n\ell j}\left|R_{n\ell j}(r)\right|^2 \tag{2}$$
$$\rho_v(r) = \frac{1}{4\pi} X_v^{n\ell j}\left|R_{n\ell j}(r)\right|^2, \tag{3}$$
where $X_{c(v)}^{n\ell j}$ refer to proton or neutron number in the sub-shell $n\ell j$ and $R_{n\ell j}(r)$ are the radial wave functions.

The distributions of matter density in Eq. (1) can be written in terms of proton $[\rho^p(r)]$ and neutron $[\rho^n(r)]$ densities as [10]:
$$\rho_m(r) = \rho^p(r) + \rho^n(r), \tag{4}$$
where $\rho^p(r)$ and $\rho^n(r)$ can be written as [10]:
$$\rho^g(r) = \rho_c^g(r) + \rho_v^g(r) \qquad g \equiv p, n \tag{5}$$
Two methods are utilized for calculating the ground state densities of exotic halo nuclei considered in the present study, which are WS+WS and HO+HO.

In the WS+WS method, the core and halo densities are described by WS radial wave function, which are taken from the solution to radial part of the Schrodinger equation using WS potential [12]:

$$\frac{\hbar^2}{2m}\frac{d^2 R_{nlj}(r)}{dr^2} + \left[\varepsilon_{nlj} - V(r) - \frac{\hbar^2}{2m}\frac{\ell(\ell+1)}{r^2}\right] R_{nlj}(r) = 0, \tag{6}$$

where $\varepsilon_{n\ell j}$ is the single-particle energy, m is the reduced mass of the core and single nucleon, and $V(r)$ is the potential of the core, given as [13]:
$$V(r) = V_0(r) + V_{so}(r)\,\boldsymbol{L}.\boldsymbol{S} + V_c(r), \tag{7}$$
where $V_0(r)$ is the central potential takes the form of WS potential [14]:
$$V_0(r) = \frac{-V_0}{1 + [e^{(r-R_0)/a_0}]} \tag{8}$$
$V_{so}(r)$ is the spin-orbit potential, expressed as [14]:

$$V_{so}(r) = V_{so} \frac{1}{r} \left[\frac{d}{dr} \frac{1}{(1 + e^{(r - R_{so})/a_{so}})} \right] \tag{9}$$

and $V_c(r)$ is the Coulomb potential (for protons only) [13]:

$$V_c(r) = \begin{cases} \dfrac{Ze^2}{r} & \text{for} \quad r > R_c \\ \dfrac{Ze^2}{R_c} \left[\dfrac{3}{2} - \dfrac{r^2}{2R_c^2} \right] & \text{for} \quad r \leq R_c \end{cases} \tag{10}$$

and $V_c(r) = 0$ for neutrons.

In the HO+HO method, the core and halo densities are described by HO single particle radial wave function, given by [15]:

$$R_{n\ell}(r) = \frac{1}{(2\ell + 1)!!} \left[\frac{2^{\ell - n + 3}(2n + 2\ell - 1)!!}{\sqrt{\pi} b^3 (n - 1)!} \right] \left(\frac{r}{b} \right)^\ell e^{-r^2/2b^2}$$
$$\sum_{k=0}^{n-1} (-1)^k \frac{(n - 1)! \, 2^k (2\ell + 1)!!}{(n - k - 1)! \, k! \, (2\ell + 2k + 1)!!} \left(\frac{r}{b} \right)^{2k} \tag{11}$$

where $b = \sqrt{\hbar / M_p \omega}$ is the HO size parameter (which is the length parameter for the HO well), M_p is the mass of the proton, and ω is the angular frequency.

The rms radii of the neutron and proton distributions can be calculated by [16]:

$$r_g = \langle r_g^2 \rangle^{1/2} = \left[\frac{\int r^2 \rho_g(r) dr}{\int \rho_g(r) dr} \right]^{1/2} \qquad g = n, p \tag{12}$$

The elastic form factors in the Plane Wave Born Approximation (PWBA) are written as [17]:

$$F(q) = \frac{4\pi}{Z} \int_0^\infty \rho_p(r) j_0(qr) r^2 dr, \tag{13}$$

where $j_0(qr)$ and q are the spherical Bessel function and momentum transfer to the target nucleus from the incident electron, respectively.

The total nuclear reaction cross section is one of the most important physical quantities characterizing the properties of nuclear reaction [18]. It is very useful for extracting fundamental information about the nuclear size and the density distributions of neutrons and protons in a nucleus. In particular, the neutron halo was found by measuring the total reaction cross section induced by radioactive nuclear beams [19, 20]. The definition of the reaction cross section and the interaction cross section are as follows [21]:

$$\sigma_R = \sigma_{tot} - \sigma_{ela} \tag{14}$$
$$\sigma_I = \sigma_R - \sigma_{inela} \tag{15}$$

where σ_{tot}, σ_{ela}, and σ_{inela} are the total reaction cross section, the elastic scattering cross section, and the inelastic scattering cross section, respectively. The reaction cross section (σ_R) can be described by subtracting the σ_{ela} from the σ_{tot}. The interaction cross section (σ_I) is the probability of the reaction in which the proton number and/or the neutron number of the projectile particle are changed. The inelastic scattering cross section is the probability of the reaction in which a projectile nucleus and/or a target nucleus is excited due to the collision. At high energy (above several hundred MeV/nucleon), it is known that the σ_R is approximated by σ_I ($\sigma_R \approx \sigma_I$) because the contribution of the inelastic scattering is low [22, 23].

In the Glauber model [24], the internal motions of the particles within the projectile (P) and target (T) are assumed slow compared to the relative motion of the centers of mass of the projectile and target. The reaction cross section for a projectile incident upon a target is given by [25]:

$$\sigma_R = 2\pi \int [1 - T(b)] \, b \, db \tag{16}$$

where $T(b)$ is the transparency function at impact parameter b.

One of the simplest methods to calculate $T(b)$ is the OLA. In this approximation, the $T(b)$ is written as the squared modulus of the elastic S-matrix for the projectile-target system [26]:

$$T(b) = \left| S_{el}^{OL}(b) \right|^2 \tag{17}$$

where

$$S_{el}^{OL}(b) = exp[iO_{PT}(b)] \tag{18}$$

$$O_{PT}(b) = \int\limits_{-\infty}^{\infty} dR_3 \int d\vec{r}_1 \int d\vec{r}_2 \rho_P(r_1)\rho_T(r_2)f_{NN}\left(|\vec{R} + \vec{r}_1 - \vec{r}_2|\right) \tag{19}$$

is the overlap of the densities of ground state for target and projectile (ρ_T and ρ_P, respectively)

3. Results and discussion

The matter, proton, and neutron densities of the ground state, the nuclear rms radii, and elastic form factors of two- neutron, ^{8}He and ^{26}F, halo nuclei are studied by the three body model of ($core + 2n$) within the HO and WS radial wave functions. Moreover, the Glauber model at high energy are used to calculate the matter rms radii and σ_R of these nuclei. The ^{8}He and ^{26}F are treated as the nuclei constituting the core of ^{6}He and ^{24}F plus two valence neutrons, respectively. The core configurations, half-life time, and separation energy (S_{2n}) [27, 28] for the considered nuclei are listed Table-1. The two valence neutrons of ^{8}He are considered to be in a pure $1p_{1/2}$ orbit, while those in ^{26}F are assumed to be in a pure $2s_{1/2}$ orbit.

The WS parameters for stable nuclei (^{4}He, ^{19}F) and the depth of WS potential (V_0) for core nucleons (protons and neutrons) as well as the depth of spin-orbit (V_{so}) of halo nuclei, ^{8}He and ^{26}F, are taken from Ref. [29]. The V_0 for outer neutron and the parameters (r_0, r_{so}, a_0 and a_{so}) are adjusted to reproduce the experimental S_n of the outer neutron and the experimental matter rms radii. We assumed that the experimental S_n of the outer neutron is equal to $S_{2n}/2$ [21]. The HO size parameters, b_c and b_v, are adjusted to reproduce the experimental rms matter radii for core (^{6}He, ^{24}F) and halo nuclei (^{8}He, ^{26}F), respectively. The parameters of WS and HO potentials used in the present analysis are listed in Table-2.

The calculated rms radii obtained by the two methods and the corresponding experimental data are summarized in Tables- 3 and 4. From the results shown in these tables, one can see clearly that the calculated rms radii are consistent with the experimental data within error bar. Table-5 exhibits the calculated single-particle energies (ε). The experimental single-particle energy is given in the last column of Table-5 for the last (valence) neutron only, due to the absence of available experimental single-particle energies for core nuclei.

Table 1- Some features for considered nuclei.

Halo nucleus	(J^π, T) [27]	Half-life time $(\tau_{1/2})$ [27]	S_{2n} (MeV) [28]	Core configuration
^{8}He	$0^+, 2$	$119.1\ ms$	$S_{2n}=2.125$	$\{(1s_{1/2})^4, (1p_{3/2})^2\}$
^{26}F	$1^+, 4$	$8.2\ ms$	$S_{2n}=5.04$	$\{(1s_{1/2})^4, (1p_{3/2})^8, (1p_{1/2})^4, (1d_{5/2})^7, (1d_{3/2})^1\}$

Table 2- Parameters of the WS and HO potentials used in the present work

Nuclei	V_0 (MeV) Core	Valence	V_{so} (MeV)	$a_0 = a_{so}$ (fm)	$r_0 = r_{so}$ (fm)	r_c (fm)	b (fm) b_c	b_v
^{8}He	50.784	40.860	6.0	0.493	1.398	1.511	1.65	2.45
^{26}F	51.198	33.150	6.0	0.536	1.403	1.357	1.82	2.91
^{4}He	73.253		6.0	0.215	1.218	1.346	1.371	
^{19}F	62.515		6.0	0.538	1.282	1.392	1.758	

Table 3-Proton and neutron rms radii for the selected nuclei

Nuclei	$\langle r_p^2 \rangle^{1/2}$		$\langle r_p^2 \rangle_{exp}^{1/2}$ [30]	$\langle r_n^2 \rangle^{1/2}$		$\langle r_n^2 \rangle_{exp}^{1/2}$ [31]	$\langle r_n^2 \rangle^{1/2} - \langle r_p^2 \rangle^{1/2}$	
	WS	HO		WS	HO		WS	HO
[8]He	2.01	2.02	2.16±0.14	2.89	2.93	2.82±0.03	0.88	0.91
[26]F	2.95	2.74	----	3.37	3.43	3.53±0.17	0.42	0.69

Table 4-Core and matter rms radii for the selected nuclei

Nuclei	$\langle r_{core}^2 \rangle^{1/2}$		$\langle r_{core}^2 \rangle_{exp}^{1/2}$ [31, 32]	$\langle r_m^2 \rangle^{1/2}$		$\langle r_m^2 \rangle_{exp}^{1/2}$ [31, 33]
	WS	HO		WS	HO	
[8]He	2.30	2.23	2.30±0.07	2.70	2.73	2.70±0.03
[26]F	3.07	2.97	3.03±0.06	3.23	3.23	3.23±0.13

Table 5-The calculated single-particle energies

Nuclei	$n\ell_j$	proton	neutron	
		ε_{cal} (MeV)	ε_{cal} (MeV)	$\varepsilon_{exp.}$ (MeV) [28]
[8]He	$1s_{1/2}$	26.612	27.239	-----
	$1p_{3/2}$	-----	11.246	-----
	$1p_{1/2}$	-----	1.062	1.062
[26]F	$1s_{1/2}$	35.196	38.976	-----
	$1p_{3/2}$	25.224	28.751	-----
	$1p_{1/2}$	23.335	26.894	-----
	$1d_{5/2}$	14.251	17.542	-----
	$1d_{3/2}$	-----	13.568	-----
	$2s_{1/2}$	-----	2.52	2.52

Figure-1 presents the calculated matter (dashed-red curve), core (green curve), and halo (dark-blue curve) densities as well as the experimental data of matter densities (shaded region) [30, 34] for [8]He (upper part) and [26]F (bottom part). The left and right panels correspond to the calculated results obtained by WS+WS and HO+HO methods, consecutively. We note that the long tail behavior (which is a distinctive feature of halo nuclei) is revealed in all dashed-red curves of Figures- 1(a)-1(d). Moreover, the dashed- red curves in Figures- 1 (a) and 1(c) are better describing the experimental data than those in Figures- 1 (b) and 1(d).

The calculated matter (dashed-red curve), proton (green curve), and neutron (dark-blue curve) densities for [8]He and [26]F obtained with two density parameterizations are plotted in Figure-2. The long tail performance is clearly noticed in the blue curves. This performance is associated to the existence of the outer two-neutron in the halo orbits. The steep slope performance is obviously observed in the green curves due to the absence of protons in the halo orbit, where all protons of these nuclei are found in its core only. Moreover, the difference between the calculated neutron and proton rms radii for the selected halo nuclei is given in Table-3. This difference provides an additional evidence for the halo structure of these nuclei.

In Figure-3, the density distribution of matter for unstable exotic [8]He and [26]F nuclei are compared with those for their stable [4]He and ^{19}F isotopes. In the figure, the dashed-red and dark-blue curves are the density distributions of matter for unstable and stable nuclei, consecutively. It is noted that the

matter density distributions for each pair of isotopes are different. The weak binding of the outer neutron in exotic ^{8}He and ^{26}F nuclei leads to the extended matter density distributions in them.

The elastic longitudinal C0 form factors of exotic ^{8}He and ^{26}F nuclei (red curves), calculated by PWBA using the proton densities, are compared in Figure-4 with those for their stable ^{4}He and ^{19}F isotopes (dark-blue curves) together with the experimental data (dark-blue symbol) of stable isotopes [32, 35]. We note that the form factors for each isotopes pair are quite different although they have the same proton number. The red and dark-blue curves in Figure- 4 (a) have no diffraction minimum throughout all range of q, while for those in Figure- 4 (b), each has one diffraction minimum. The minima position of ^{26}F (red curve) has left shift as compared with that of ^{19}F (dark-blue curve). This change is attributed to the variation in the proton densities due to the presence of the extra neutrons.
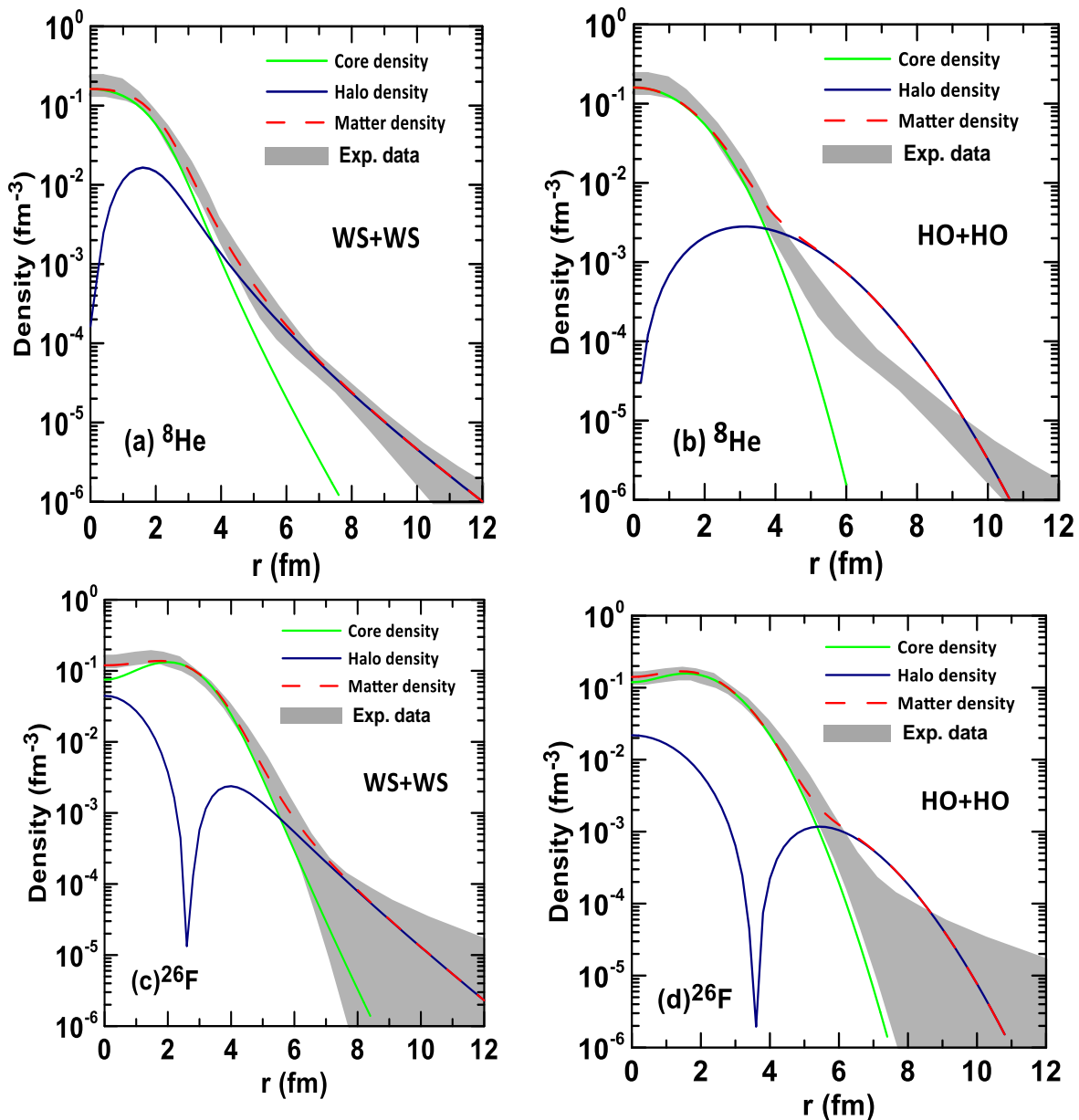

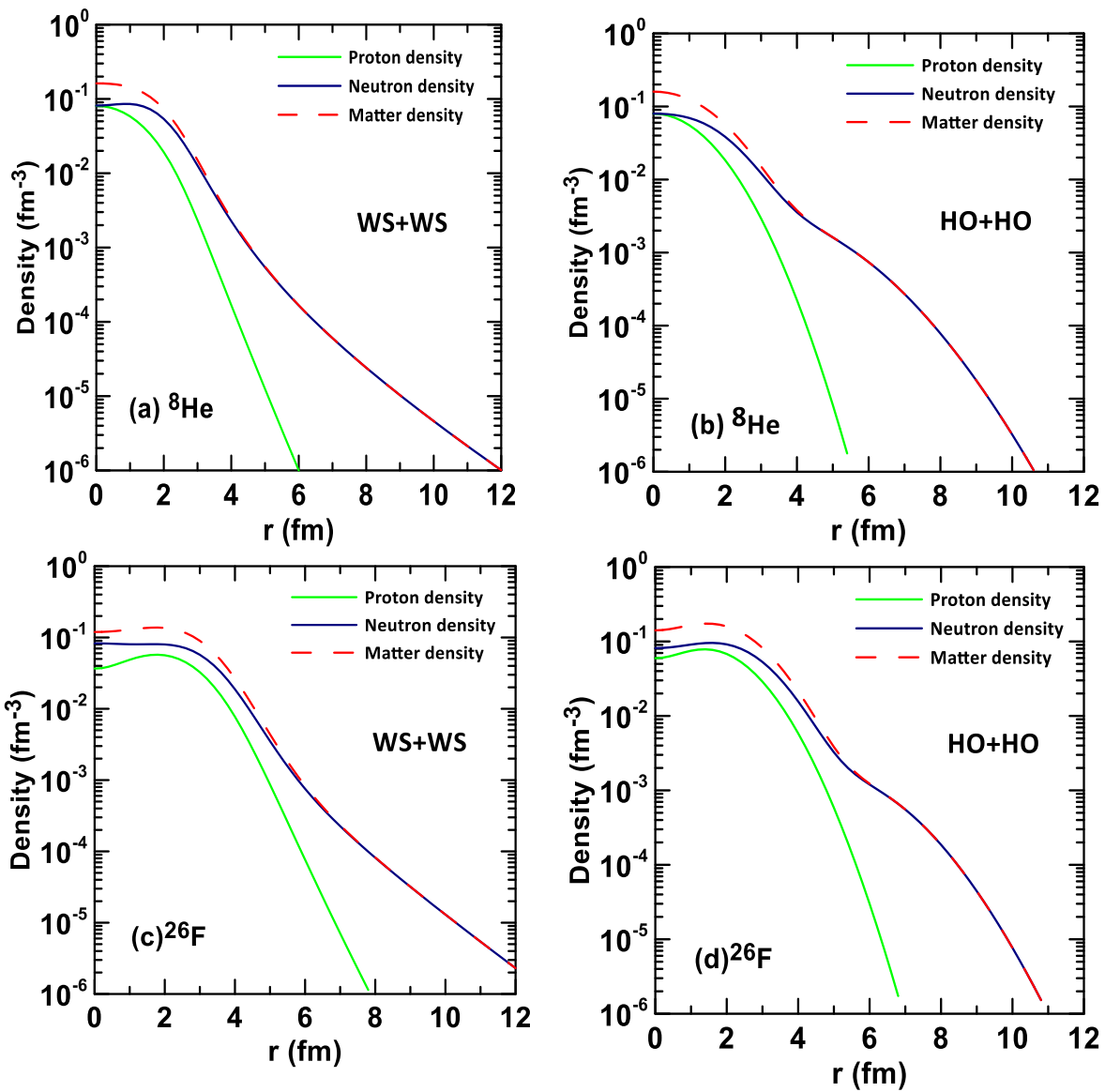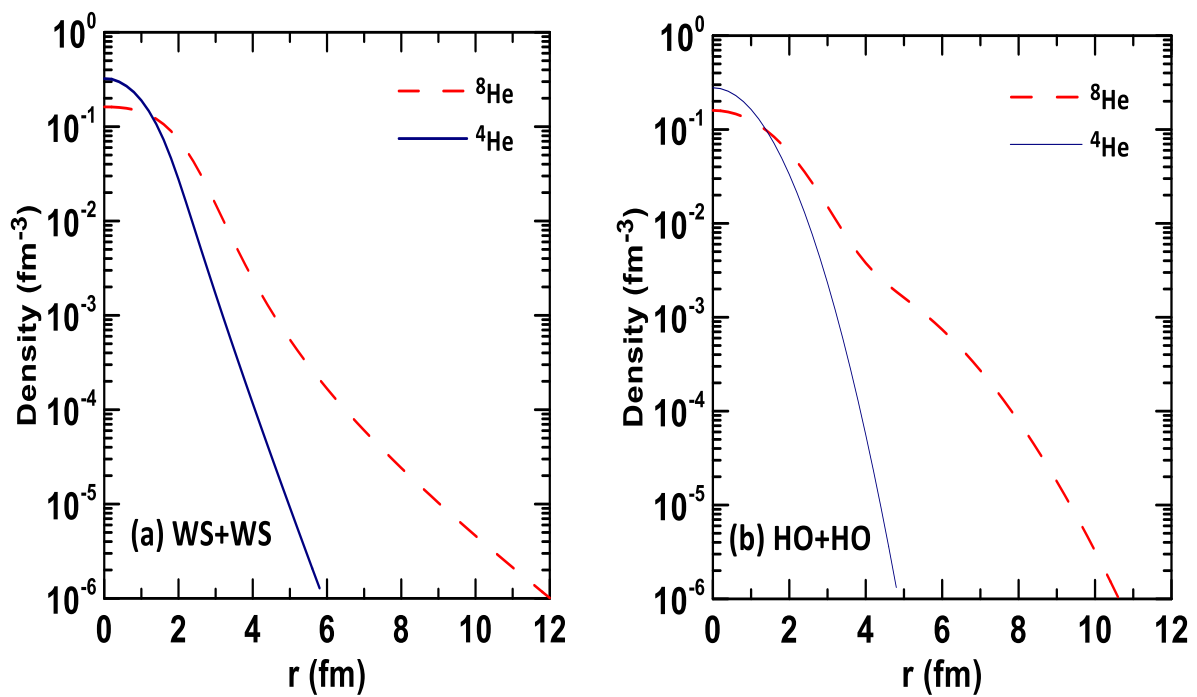**Figure 1**-The matter, core, and halo densities for halo nuclei ^{8}He and ^{26}F.

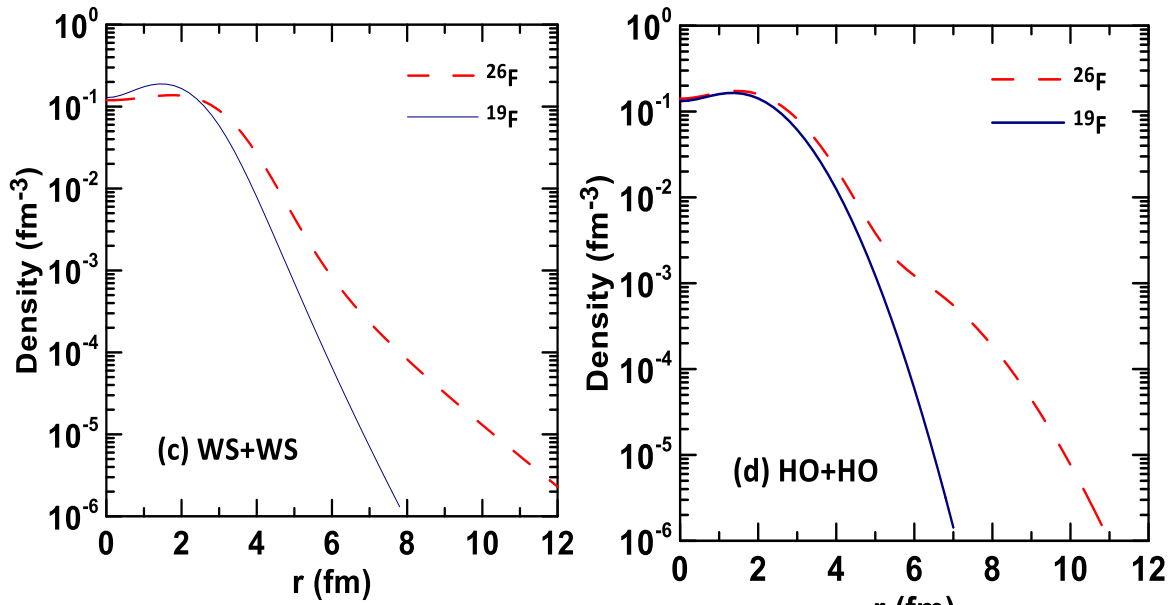**Figure 2**- The matter, proton, and neutron densities for halo nuclei ^{8}He and ^{26}F

Figure 3- Calculated matter densities for nuclei ^{4,8}He and ^{19,26}F.

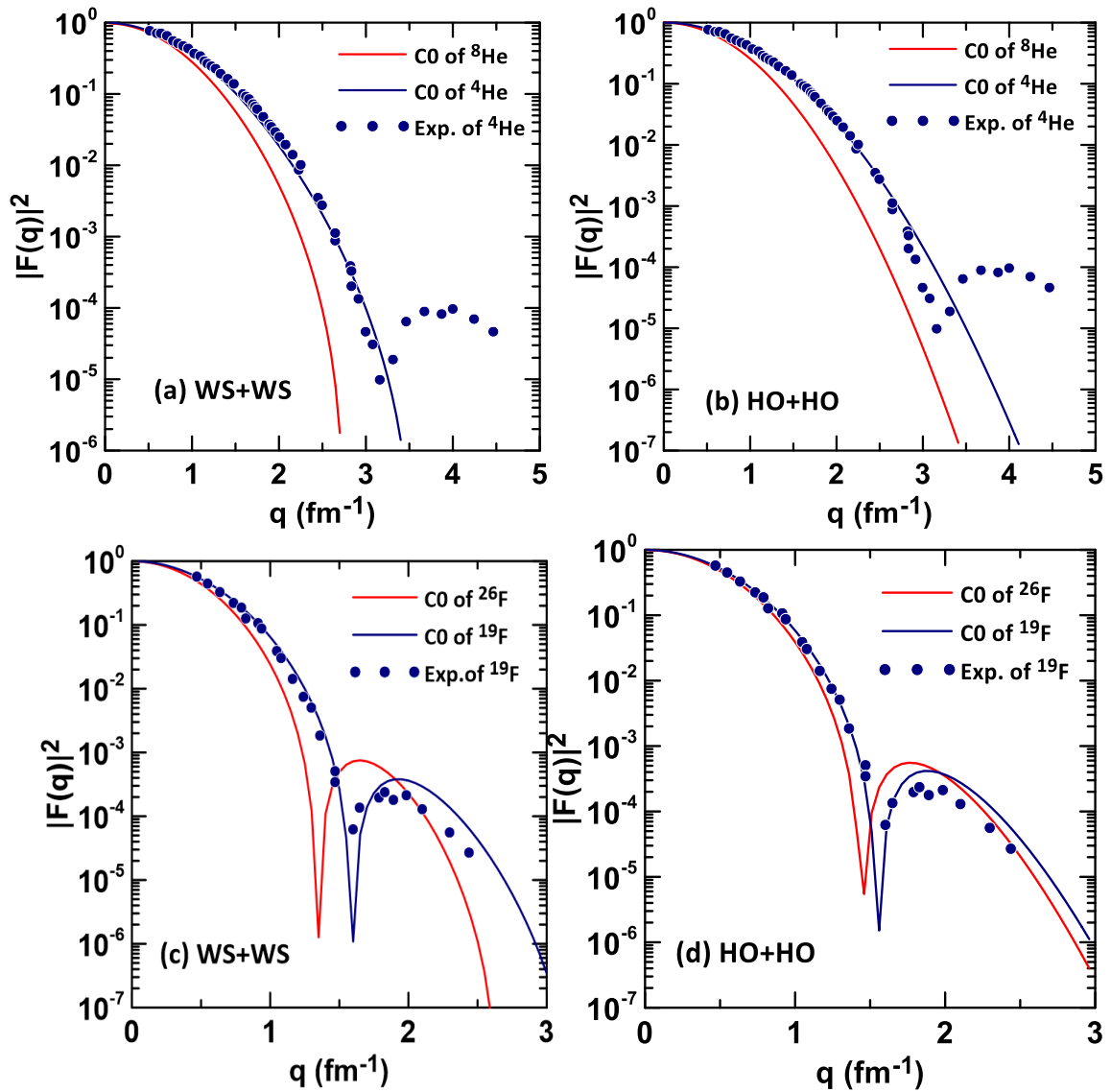**Figure 4**- Elastic form factors for nuclei ^{4,8}He and ^{19,26}F.

The calculated σ_R at high energy for ^{8}He + ^{12}C and ^{26}F + ^{12}C systems using the Glauber model with OLA along with experimental data are listed in Table 5. From the results, one can see clearly that a good description of the experimental σ_R is obtained by the calculated results for both halo nuclei.

Table 5-Calculated and experimental σ_R for ^{8}He + ^{12}C and ^{26}F + ^{12}C systems.

Halo nuclei	Energy (MeV) [31]	Calculated σ_R (mb)	Experimental σ_R (mb) [31]
^{8}He	790	820	817±6
^{26}F	950	1365	1353±54

To calculate the matter rms radius of halo nuclei from the reaction cross sections (σ_R), the calculated σ_R (red line) obtained by the Glauber model within OLA versus the matter rms radii for the halo nuclei, ^{8}He and ^{26}F, on ^{12}C target at high energy are plotted in Figures- 5(a) and 5(b), consecutively. The horizontal black line shows the experimental σ_R (given in Table-5) with error bar plotted by the shaded area. The intersection point of the red line with horizontal black line represents the obtained matter rms radius ($\langle r_m^2 \rangle^{1/2}$) for the halo nuclei. From Figure- 5(a) [Figure- 5(b)] we show that the calculated $\langle r_m^2 \rangle^{1/2}$ for ^{8}He [^{26}F] is equal to 2.67 [3.21] fm, which agree well with the analogous experimental data of 2.70±0.03 [3.23±0.13] fm.

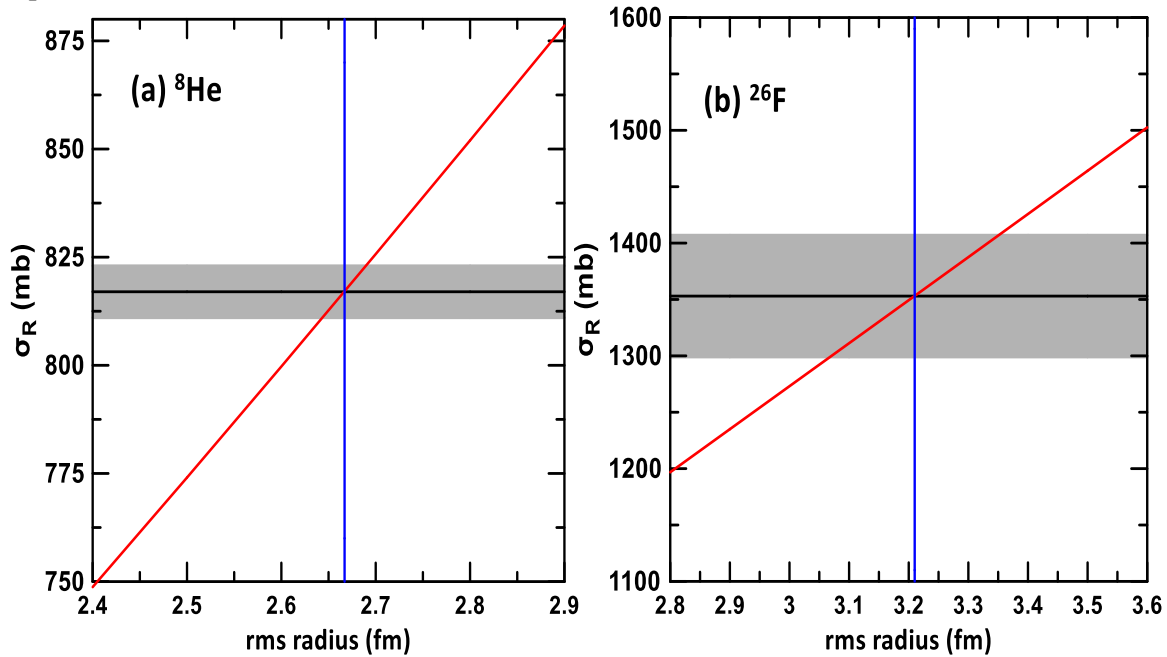**Figure 5-**The reaction cross section versus the matter rms radii for the halo nuclei ^{8}He and ^{26}F.

4. Summary and conclusions
The matter, proton, and neutron densities of the ground state, the nuclear rms radii, and elastic form factors of two- neutron, ^{8}He and ^{26}F, halo nuclei have been studied by the three body model of $(core + 2n)$ within the HO and WS radial wave functions. Moreover, the Glauber model at high energy has been used to calculate the rms radii and reaction cross section of these nuclei. The calculated results lead to several conclusions.
It was found that both the HO and WS radial wave functions within the three body model are capable of providing theoretical predictions on the structure of exotic (halo) nuclei and are in a satisfactory description with those of experimental data.
The halo structure of these exotic nuclei is emphasized through exhibiting the long tail performance in their calculated neutron and matter density distributions, where this performance is considered as a distinctive feature of halo nuclei.

A supplementary support for the halo structure of these exotic nuclei was found due to the noticeable difference between the calculated overall neutron and proton rms radii.

4- The two halo neutrons in ^{8}He have a pure $(1p_{1/2})^2$ configuration while those for ^{26}F have a pure $(2s_{1/2})^2$ configuration.

It was found that the major difference between the calculated form factor of the unstable nuclei, ^{8}He and ^{26}F, and those of their stable isotope, ^{4}He and ^{19}F, is attributed to the variation in the proton densities due to the presence of the extra neutrons.

The Glauber model at high energy gives a good description for both matter rms radii and σ_R of these nuclei.

References
1. I. Tanihata. **1996.** *J. Phys. G: Nucl. Part. Phys.* **22**: 157.
2. P. G. Hansen *et al*. **1995**. *Ann. Rev. Nucl. Part. Sci.***45**: 591.
3. B. Q. Chen *et al*. **1998**. *J. Phys. G: Nucl. Part. Phys*. **24**: 97.
4. Z. Z. Ren *et al*. **1998**. *Phys. Rev. C* **57**: 2752.
5. R. Morlock *et al*. **1997**. *Phys. Rev. Lett.* **79**: 3837.
6. A. Navin *et al*. **1998**. *Phys. Rev. Lett.* **81**: 5089.
7. C. B. Qiu and M. Z. Yu. **2001**. *Chin. Phys. Lett.* **18**: 1561.
8. Z. Y. Lin *et al*. **2003**. *Chin. Phys. Lett.* **20**: 53.
9. A. A. Alzubadi, N. F. Latooffi and R. A. Radhi. **2015**. *Int. J. Mod. Phys. E* **24**: 1550099.
10. A. N. Abdullah. **2020**. *Int. J. Mod. Phys. E,* **29**: 2050015.
11. G. D. Alkhazov, I. S. Novikov and Y. M. Shabelski. **2011**. *Int. J. Mod. Phys. E,* **20**:583.
12. W. Meng *et al*. **2008**. *Chin. Phys. C,* **32**: 548.
13. Y. Chu, Z. Z. Ren and C. Xu. **2008**. *Eur. Phys. J. A,* **37**: 361.
14. A. N. Abdullah. **2017**. *Int. J. Mod. Phys. E,* **26**: 1750048.
15. P. J. Brussard and P. W. M. Glaudemans.**1977**. "*Shell-Model Application in Nuclear spectroscopy*", North-Holland, Amesterdam.
16. L. G. Qiang. **1991**. *J. Phys. G. Nucl. Part. Phys.* **17**: 1.
17. A. N. Antonov *et al*. **2004**. *Int. J. Mod. Phys. E,* **13**: 759.
18. C. Xiangzhou, *et al.* **1998**. *Phys. Rev. C,* **58**: 572.
19. I. Tanihata *et al*. 1985. *Phys. Rev. Lett.* **55**: 2676.
20. I. Tanihata, D. Hirata, T. Kobayashi, S. Shimoura, K. Sugimoto, and H. Toki. **1992**. *Phys. Lett. B* **289**: 261.
21. T. Moriguchi. **2011**. Ph.D. Thesis, University of Tsukuba.
22. Y. Ogawa et al. **1992**. *Nucl. Phys. A,* **543**:722.
23. A. Ozawa et al., **2002**. *Nucl. Phys. A,* **709**: 60.
24. J. A. Tostevin *et al*. **1998**. *Nucl. Phys. A,* **630**: 340c.
25. T. Zheng *et al*. **2002**. *Nucl. Phys. A* **709**: 103.
26. J. A. Tostevin and J. S. Al-Khalili. **1997**. *Nucl. Phys. A,* **616**: 418c.
27. M. Wang *et al*. **2017**. *Chin. Phys. C,* **41**: 030003.
28. G. Audi *et al*. **2017**. *Chin. Phys. C,* **41**: 030001.
29. B. A. Brown and W. D. M. Rae. **2014**. *Nucl. Data Sheets,* **120**: 115.
30. M. Tanaka *et al*. **2015**. *JPS Conf. Proc.* **6**: 020026.
31. S. Ahmad *et al*. **2017**. *Phys. Rev. C,* **96**: 064602.
32. A. N. Antonov *et al*. **2005**. *Phys. Rev. C,* **72**: 044307.
33. I. Tanihata *et al*. **1985**. *Phys. Rev. Lett.* **55**: 2676.
34. A. Ozawa. **2002**. *Eur. Phys. J. A,* **13**: 163.
35. P. L. Hallowell *et al*. **1973**. *Phys. Rev. C,* **7**:1396.